Journal of Power Sources 188 (2009) 230–237

Contents lists available at ScienceDirect

Journal of Power Sources

journal homepage: www.elsevier.com/locate/jpowsour

Structural and electrochemical characterisation of $Pr_{0.7}Ca_{0.3}Cr_{1-y}Mn_yO_{3-\delta}$ as symmetrical solid oxide fuel cell electrodes

Abdelouhad El-Himri[a,b], David Marrero-López[a], Juan Carlos Ruiz-Morales[a], Juan Peña-Martínez[a], Pedro Núñez[a,*]

[a] Department of Inorganic Chemistry and Institute of Materials and Nanotechnology (IMN), University of La Laguna, 38200 Tenerife, Spain
[b] Université Cadi Ayyad, Faculté Polydisciplinaire, Département des Sciences de la Matière-Chimie, Safi, Maroc

ARTICLE INFO

Article history:
Received 22 August 2008
Received in revised form 26 October 2008
Accepted 16 November 2008
Available online 21 November 2008

Keywords:
SOFC
Symmetrical fuel cell
Symmetrical electrodes
Chromium-manganite
YSZ

ABSTRACT

A series of compounds with composition $Pr_{0.7}Ca_{0.3}Cr_{1-y}Mn_yO_{3-\delta}$ ($y = 0.2$, 0.4, 0.6, 0.8) were prepared from an alternative freeze-drying precursor method to obtain polycrystalline powders at relatively low temperature. These perovskite-type materials were tested simultaneously as both anode and cathode in a symmetrical SOFC. The effect of the ratio Mn/Cr on the structure, microstructure and electrochemical properties was studied. The performance is rather modest at low temperature and only interesting values were obtained at high temperatures. An assembled symmetrical SOFC rendered performances of 250 and 160 mW cm^{-2}, at 950 °C, under humidified H_2 and CH_4 respectively.

1. Introduction

A typical solid oxide fuel cell (SOFC) is an electrochemical device made of three main ceramic components, i.e. an anode, a cathode and a solid electrolyte. The state-of-the-art solid electrolyte, cathode and anode materials at high temperature are yttria-stabilised zirconia (YSZ), lanthanum strontium manganate $La_{1-x}Sr_xMnO_{3-\delta}$ (LSM) and Ni/YSZ cermet respectively. Regarding the anode material, the Ni/YSZ cermet material presents mixed ionic-electronic conductivity and excellent catalytic properties for fuel oxidation. All of them should fulfilled some general and specific requirements to be properly used in a SOFC, such as phase stability and compatibility with the other cell components [1,2].

An alternative approach to this configuration is to use simultaneously the same material as both anode and cathode. This symmetrical configuration is typical in the polymeric electrolyte membrane fuel cells (PEMFCs), where the electrode material is usually Pt-C with high content of Pt, therefore the cost of these devices is a drawback. On the contrary, SOFCs have high versatility on the election of electrode materials, e.g. mixture oxides, cermets, etc. Symmetrical solid oxide fuel cells (SSOFC) present several advantages compared to conventional SOFCs, because the number of cell components are reduced facilitating the assembly of a fuel cell in a single thermal treatment and minimising compatibility requirements [3,4]. Furthermore, this configuration could overcome two of the main drawbacks associated to SOFC technology when operating directly with hydrocarbon fuels, i.e. reversible sulphur poisoning and carbon deposition, due to the possibility – despite the engineering issue – to reverse the gas flow oxidising any sulphur specie or C-deposit and hence recovering any loss of performance.

There has been a growing interested in the last few years in the research of potential symmetrical electrode materials for SOFC applications [3–12]. The requirements for candidate symmetrical electrode materials are rather restrictive as they should include all the conditions applicable to an anode and cathode simultaneously [3]. Thus the symmetrical electrode must operate as a cathode under oxidising conditions and an anode under reducing conditions. The typical performances obtained from SSOFCs are somewhat lower compared to traditional Fuel Cell due to the extreme difficult to find a perfect material that fulfils all the requirements. The SSOFC concept has been already proved with several materials such as: chromites, chromium-manganites, titanates activated under oxidising conditions and its composites with electrolytes as YSZ and gadolinium-doped ceria (CGO) [3–12]. The chromites generally used as interconnects fulfil almost all the conditions required for a potential symmetrical electrode material. The main problem of the chromites is related to their rather modest catalytic activity towards hydrocarbon oxidation [13,14], although

* Corresponding author at: Avda. Astrofisico Fco. Sanchez s/n, E-38200 La Laguna, Tenerife, Spain. Tel.: +34 922318501; fax: +34 922318461.
E-mail address: pnunez@ull.es (P. Núñez).

0378-7753/$ – see front matter © 2008 Elsevier B.V. All rights reserved.
doi:10.1016/j.jpowsour.2008.11.050

this activity can be enhanced by partial substitution of chromium for manganese [15–18].

On the other hand, La-based chromites have a structural transformation from orthorhombic to rhombohedral at high temperature, which can be detrimental for practical applications [19]. Nevertheless, the substitution of Pr by La shifts this transformation below room temperature [20]. Furthermore, Ca-doping in the A-site of the perovskite helps to reduce the thermal expansion mismatch between the oxidised and reduced form of the La-based chromite [1].

In the communication presented herein, the electrochemical properties and potential use of $Pr_{0.7}Ca_{0.3}Cr_{1-y}Mn_yO_{3-\delta}$ ($y = 0.2, 0.4, 0.6, 0.8$) as symmetrical SOFC electrodes have been studied. An alternative synthetic route based on freeze-dried precursors was used to obtain powders of submicrometric particle size at low temperature and to avoid the formation of secondary phases, which usually appears by conventional solid state reaction method.

2. Experimental

2.1. Synthesis of electrode

Polycrystalline materials with composition $Pr_{0.7}Ca_{0.3}Cr_{1-y}Mn_yO_{3-\delta}$ ($x = 0.2, 0.4, 0.6, 0.8$) were prepared by the traditional ceramic method and also by a modified freeze-dried precursor method using ethylenediaminetetraacetic acid (EDTA) as complexing agent.

The ceramic route was carried out by ball-milling stoichiometric amounts of Pr_6O_{11} (99.9%, Aldrich), $CaCO_3$ (99.9%, Aldrich), MnO (99%, Aldrich) and Cr_2O_3 (99.9%, Aldrich) in acetone using a Fritsch P-7 planetary ball mill with zirconia vessel and balls at 150 rpm for 2 h. The resulting mixture was dried and fired in air up to 1200 °C for 12 h and further ground. A final thermal treatment at 1400 °C was necessary to obtain a single phase.

The reagents used in the freeze-drying method were $Pr(NO_3)_3{\cdot}6H_2O$ (99.99%, Aldrich), $Ca(NO_3)_3{\cdot}4H_2O$ (99.0%, Aldrich), $Cr(NO_3)_3{\cdot}9H_2O$, (99.0%, Aldrich) and $Mn(CH_3COO)_2{\cdot}4H_2O$, (Aldrich, 99.9%). Stoichiometric cation solutions containing Pr, Ca, Cr and Mn were prepared by dissolving their respective salts in distilled water. These solutions were mixed and EDTA was added in a relation ligand:metal of 1:1 to obtain a homogeneous and transparent solution without any visible formation of precipitation. Droplets of these solutions were flash frozen by projection on liquid nitrogen retaining the cation homogeneity of the starting solution. The frozen drops were freeze-dried at a pressure of 1–10 Pa in a Heto Lyolab freeze-dryer for 3 days. In this way, dried and amorphous solid precursors were obtained. The amorphous precursors were heated in air at 5 °C min^{-1} up to 1000 °C for 12 h and finally cooled down at 5 °C min^{-1} to room temperature.

The samples $Pr_{0.7}Ca_{0.3}Cr_{1-y}Mn_yO_{3-\delta}$ are hereafter labelled as $PCCM_y$ as a function of the Mn-content.

2.2. X-ray characterisation

X-ray powder diffraction (XRD) patterns were acquired using a Philips X'Pert Pro diffractometer, equipped with a Ge(1 1 1) primary monochromator and an X'Celerator detector. XRD patterns were collected with a scanning step of 0.016° over the angular 2θ range 20–100° with a collection time of 2 h. Structure refinements were performed using the FullProf software [21]. All the graphical representations concerning XRD patterns were performed using WinPlotr program [22].

2.3. Stability and chemical compatibility

The phase stability of the materials under reducing conditions was investigated up to 950 °C flowing 5%H_2-Ar for 24 h. Chemical compatibility tests were performed to determine the stability of the electrodes in contact with the electrolyte. For this purpose, powder mixtures of PCCM and YSZ in relation 1:1 (%wt.), were ground and fired at 950 °C in air and 5%H_2-Ar for 24 h. The materials were then characterised by XRD to investigate the presence of any degradation or reaction products.

2.4. Conductivity measurements of the electrodes

Polycrystalline powders were uniaxially pressed into disks of 7 mm of diameter at 130 MPa. Dense pellets with relative density higher than 95% were obtained after sintered at 1400 °C for 10 h. Pellets with very high geometrical factor (thickness = 3 mm and diameter = 5 mm) were prepared to enhance the pellet resistance and to be able to use the impedance spectroscopy. All samples were prepared in the same conditions to compare the electrical results. The pellet was fixed in an electrochemical setup of alumina with Pt-wires for the electrical connections and then inserted into a quartz flow-through tube furnace. Impedance spectra (IS) under air and humidified 5%H_2-Ar atmospheres were obtained using a Solartron 1260 impedance analyser in the frequency range 10^{-1} to 10^6 Hz, with an ac perturbation voltage of 100 mV for the temperature range 400–950 °C. The conductivity values of some samples were also measured by the Van der Pauw's four probe method to compare with the results obtained by IS, rendering similar results by both methods.

2.5. Area-specific resistance (ASR) from symmetrical measurements

Area-specific resistance measurements were carried out by impedance spectroscopy on a 2-electrode arrangement [4], using ~1.5 mm thickness and ~20 mm diameter YSZ dense pellets as electrolyte. Dense YSZ pellets were obtained after uniaxially pressing 8%-YSZ (Pikem) powders at 200 MPa and then sintered at 1500 °C for 10 h.

A slurry of the electrode powder was prepared using Decoflux™ (WB41, Zschwimmer and Schwartz) as binder in a weight ratio powder:binder of 1:1 and a thin film of the slurry was coated onto both surfaces of the electrolyte and then fired at 1200 °C in air for 2 h. Current collector was formed by coating platinum paste on both sides of the pellets and then fired at 950 °C in air for 2 h to ensure good adherence. The impedance spectra were measured under symmetric atmosphere (air and humidified 5%H_2-Ar) using an impedance analyser (Solartron 1260) in the frequency range 10^{-1} to 10^6 Hz and with an excitation voltage of 100 mV.

2.6. Fuel cell tests

Fuel cell tests of the YSZ-based electrolyte supported systems using PCCM as symmetrical electrode material (cathode and anode) were carried out. The thickness of the dense YSZ-electrolyte was around 370 μm. The electrode material was deposited on both sides (electrode surface of 0.49 cm^2) of YSZ pellets at 1200 °C for 2 h in air. A Pt-based ink was used to form current collectors after firing at 950 °C in air for 2 h. The cell was introduced in a fuel cell setup and sealed using a glass-ceramic-based material (Ceramabond 668, Aremco). The current–voltage characteristics of the single cells were determined by cyclic-voltammetry at a scan rate of 10 mV s^{-1} using a Zahner IM6e electrochemical analyser. Fuel cell tests were carried out using humidified 5% H_2-Ar, pure H_2 and CH_4 as fuels and air as oxidant, at temperatures ranging between 850 and 950 °C. The water content was fixed by bubbling the gas through a humidifier thermostated at 20 °C. The concentration of water at that temperature was estimated as 2.3%.

2.7. Microstructural characterisation

The morphology of the powders, sintered pellets and the electrode–electrolyte interfaces were analysed by scanning electron microscope (Jeol, JSM-6300) operating at an accelerating voltage of 20 kV. All the preparations were covered with a thin film of gold for better image definition.

3. Results and discussion

3.1. Structural characterisation

Fig. 1a and b show the XRD patterns for a representative sample with composition $PCCM_{0.6}$ prepared by conventional solid state reaction and freeze-drying method as a function of the firing temperature.

The XRD patterns for samples prepared by conventional solid state reaction between 900 and 1200 °C consist mainly in a mixture of two phases with similar structure. This is clearly visible in the inset of Fig. 1a, where all the diffraction peaks exhibit two components attributed to Mn and Cr-rich phases. A single phase is progressively formed as the temperature increases, although temperatures higher than 1200 °C are required to obtain a nearly pure phase. On the contrary, single perovskite-type structures have been synthesized by the freeze-dried precursor method after one thermal treatment at only 800–900 °C (Fig. 1b). This is an advantage to prepare polycrystalline materials with fine grain sizes, which can contribute to improve the physicochemical properties of the SOFC electrodes. Low temperature synthesis methods give rise to materials with lower grain size and better reactivity and therefore they are more appropriate for the preparation of SOFC electrodes than those obtained by conventional solid state reaction. This contributes to a reduction of the deposition temperature of the electrodes, avoiding excessive reaction in the electrolyte–electrode interface that could compromise the SOFC performance. In addition, a more homogeneous porosity is obtained, which generally results in a better diffusion of gases towards the electrodes and an increase of reaction sites, where electrochemical reaction occurs. All these factors generally contribute to enhance the electrochemical performance of the electrodes. Another issue to be considered is that freeze-dried method has several advantages compared to other alternative precursor routes. For example, in sol–gel routes, the pH, cation concentration, ligand–metal ratio and gelification temperature are critical factors to be controlled and to avoid undesirable precipitation during the gelification process. On the contrary, the only parameters that affect the freeze-dried product are: the cation concentration and the pH of the starting solution, which are easier controllable. It should be also noted that many cation-solutions are unstable and tend to precipitate in a short period (few minutes or hours), however this is prevented after the fast frozen of the solution in liquid nitrogen. It should be also considered that freeze drying is a process which is used to dehydrate in large scale a wide variety of industrial products, e.g. foods, pharmaceuticals, etc. Therefore, the preparation of large quantities of precursor for the synthesis of almost any ceramic material is possible. In fact, the use of freeze-dried precursors has proved to be a very versatile method for obtaining different materials as mixed oxides [23,24], metal nitrides [25], etc.

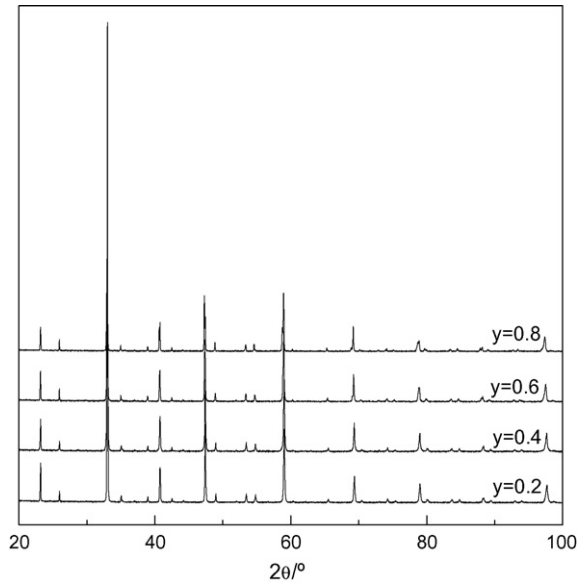

Fig. 2. XRD patterns of $Pr_{0.7}Ca_{0.3}Cr_{1-y}Mn_yO_{3-\delta}$ series prepared from freeze-dried precursors at 1000 °C.

XRD patterns for $Pr_{0.7}Ca_{0.3}Cr_{1-y}Mn_yO_{3-\delta}$ ($y = 0.2$, 0.4, 0.6 and 0.8) after thermal treatment of the respective amorphous freeze-dried precursors at 1000 °C are shown in Fig. 2. The XRD patterns

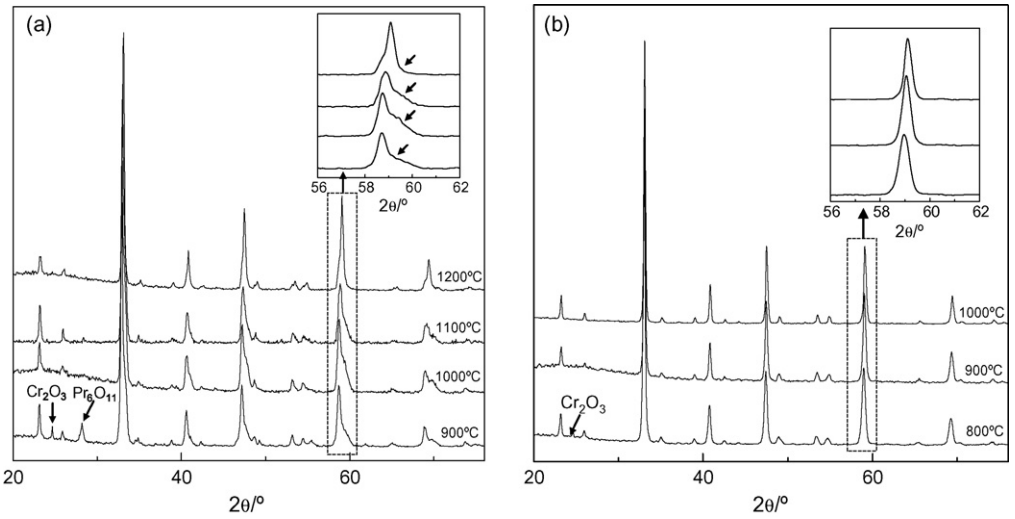

Fig. 1. Evolution of XRD patterns of $Pr_{0.7}Ca_{0.3}Cr_{0.4}Mn_{0.6}O_{3-\delta}$ prepared from (a) conventional solid state reaction and (b) freeze-dried precursor method at different temperatures. Two similar phases are observed in samples prepared by solid state reaction up to 1200 °C indicated by arrows in the inset.

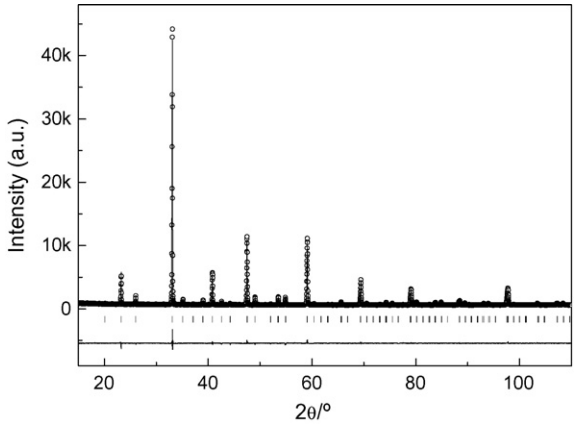

Fig. 3. Rietveld refinement of polycrystalline $Pr_{0.7}Ca_{0.3}Cr_{0.4}Mn_{0.6}O_{3-\delta}$ calcined at 1000 °C.

indicate that all the compositions are single orthorhombic phases and isostructural with $LaCrO_3$ (s.g. *Pnma*).

The structure of the $Pr_{0.7}Ca_{0.3}Cr_{1-y}Mn_yO_{3-\delta}$ phases have been refined in the space group *Pnma* from room temperature X-ray diffraction data, using the Rietveld method. The starting structural model was that of $LaCrO_3$. The fits were performed using a pseudo-Voigt peak-shape function. In the final runs, usual profile parameters (scale factors, background coefficients, zero-points, half-width, pseudo-Voigt, asymmetry parameters for the peak-shape and atomic positions) were refined. The results of the Rietveld refinement for $PCCM_{0.6}$ sample are shown in Fig. 3. The crystallographic parameters for all the composition are listed in Table 1. The main effect of substitution of Cr by Mn in $Pr_{0.7}Ca_{0.3}Cr_{1-y}Mn_yO_3$ is a slight expansion of the unit cell volume without any appreciable structural change detectable by XRD in the whole compositional range studied $0.2 \leq y \leq 0.8$. Moreover, the R-factors obtained in the Rietveld refinement are similar for all compositions.

3.2. Chemical compatibility and redox stability

Fig. 4 shows the XRD patterns corresponding to individual YSZ and $PCCM_{0.6}$ at room temperature and 1:1 wt.% PCCM:YSZ composites calcined at 950 °C for 24 h and 1200 °C for 2 h. After calcined at 950 °C the main diffraction peaks do not shift significantly and moreover there are no extra diffraction peaks, which may indicate that no significant reaction occur between the electrolyte and the electrode materials.

Although no degradation of PCCM electrodes was observed in air conditions, it should be pointed out that under fuel cell working conditions a decrease of performance is observed during the time when the Mn content is higher than 50%. Redox stability studies were performed exposing the powder electrodes under dry 5%H_2-Ar flow for 24 h at 950 °C. The XRD patterns of the reduced phases are shown in Fig. 5. No apparent degradation or phase transformation is observed for samples with Mn content $y \leq 0.4$ after annealing under these conditions. However, a significant loss of crystallinity is observed for samples with higher Mn content ($y \geq 0.6$) as can be observed in the diffraction peak broadening in Fig. 5. This crystallinity loss is due to some grade of amorphisation in the material, possibly because of an excessive reduction and oxygen losses and it seems to explain the decrease of efficiency during the fuel cell operation. Another issue to be considered is that these electrode materials do not exhibit any structural transformation during reduction, contrary to the lanthanum chromium-manganite, $La_{0.75}Sr_{0.25}Cr_{0.5}Mn_{0.5}O_{3-\delta}$ [26].

Table 1
Crystallography parameters of $Pr_{0.7}Ca_{0.3}Cr_{1-y}Mn_yO_{3-\delta}$ (y = 0.2, 0.4, 0.6, 0.8) series obtained by XRD Rietveld refinement.

	y = 0.8	y = 0.6	y = 0.4	y = 0.2
a (Å)	5.4507(1)	5.4359(9)	5.4238(1)	5.4228(1)
b (Å)	7.6712(2)	7.662(1)	7.6532(1)	7.6513(1)
c (Å)	5.4279(1)	5.4204(9)	5.4127(1)	5.4099(1)
V (Å^3)	226.96(8)	225.76(7)	224.68(7)	224.46(7)
Pr (4c)/Ca				
x	0.0325(2)	0.0306(2)	0.0296(2)	0.0301(2)
y	0.25	0.25	0.25	0.25
z	0.0102(4)	0.0092(3)	0.0088(4)	0.0091(3)
B	1.30(3)	1.47(2)	1.65(3)	1.37(3)
Occ	0.7	0.7	0.7	0.7
Cr (4b)/Mn				
x	0	0	0	0
y	0	0	0	0
z	0.5	0.5	0.5	0.5
B	1.48(5)	1.41(4)	1.58(4)	1.37(3)
Occ	0.2	0.4	0.6	0.8
O1(4c)				
x	0.485(2)	0.488(2)	0.486(2)	0.488(2)
y	0.25	0.25	0.25	0.25
z	−0.066(3)	−0.062(3)	−0.076(4)	−0.066(4)
B	2.2(3)	1.8(1)	1.6(1)	1.37(1)
Occ	1	1	1	1
O2(8d)				
x	0.281(2)	0.289(9)	0.294(3)	0.291(2)
y	0.033(1)	0.031(1)	0.025(2)	0.028(1)
z	−0.292(2)	−0.293(2)	−0.293(3)	−0.298(2)
B	2.3(2)	1.8(1)	1.7(1)	1.3(1)
Occ	1	1	1	1
R_{wp} (%)	18.0	15.4	17.4	14.6
R_{exp} (%)	11.3	11.0	11.3	10.8
R_B (%)	15.6	8.5	9.9	7.9

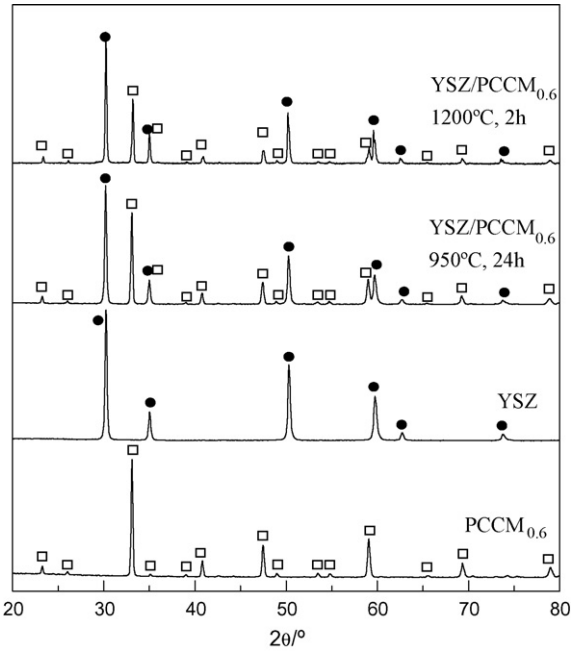

Fig. 4. XRD patterns for $PCCM_{0.6}$ and YSZ at room temperature and composite of PCCM-YSZ after fired at 950 °C for 24 h and 1200 °C for 2 h.

3.3. Overall conductivity

The Nyquist plots of dense PCCM ceramics only show the presence of inductive effects indicating predominant electronic contribution in this material. The overall resistance, under both air and 5%H_2-Ar conditions, was obtained from the high frequency Z'-intercept. The values obtained, Fig. 6, are comparable to those reported in the literature for similar compositions [19]. The Arrhenius plot of the overall conductivity for a representative sample with composition $PCCM_{0.6}$ is shown in Fig. 6a. A lineal dependence is observed in the temperature range studied 400–950 °C, which indicates a thermally activated hopping polaron mechanism, with an activation energy of 0.094 and 0.49 eV under air and 5%H_2-Ar atmospheres, respectively. The lower conductivity under reducing

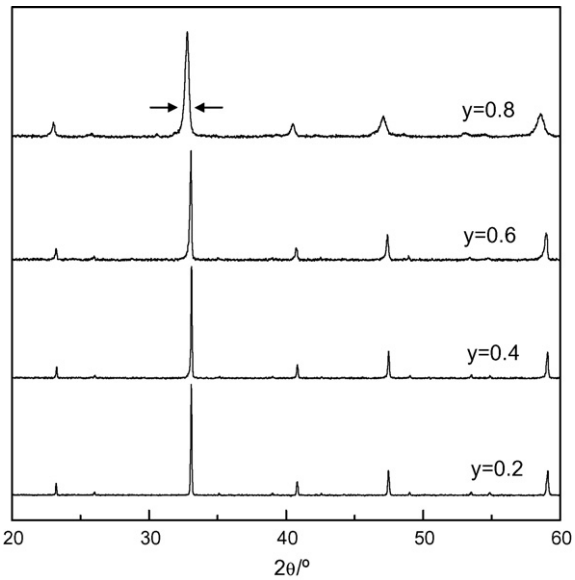

Fig. 5. XRD patterns of $Pr_{0.7}Ca_{0.3}Cr_{1-y}Mn_yO_{3-\delta}$ samples after annealed under 5%H_2-Ar for 2 h at 950 °C.

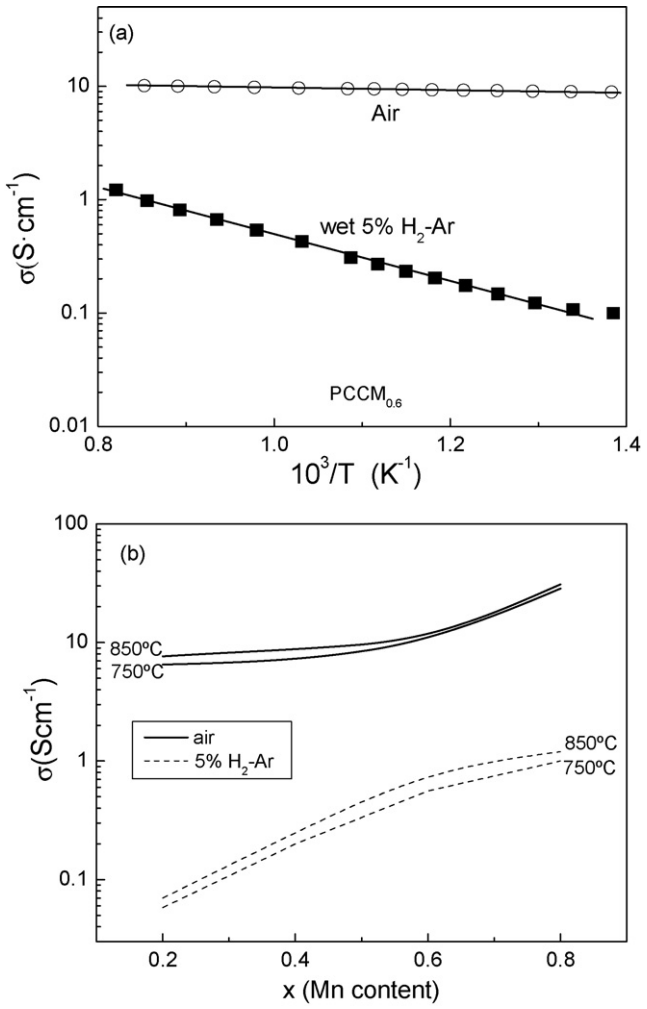

Fig. 6. Arrhenius plot of the overall conductivity for a representative sample with composition $Pr_{0.7}Ca_{0.3}Cr_{0.4}Mn_{0.6}O_{3-\delta}$ (a). Variation of the overall conductivity for $Pr_{0.7}Ca_{0.3}Cr_{1-y}Mn_yO_{3-\delta}$ series as a function of the Mn-content at 750 and 850 °C (b).

conditions evidences that these perovskites exhibit a predominant p-type electronic conductivity with a behaviour similar to (La,Sr)(CrMn)O_3 anodes. The lower conductivity values under low oxygen partial pressure are due to Mn reduction and the consequently oxygen losses that causes a reduction of the charge carrier concentration, thus decreasing the electronic conductivity from 10 S cm^{-1} in air to 1 S cm^{-1} in humidified 5%H_2-Ar for $PCCM_{0.6}$. On the other hand, the dependence of the overall conductivity in $Pr_{0.7}Ca_{0.3}Cr_{1-y}Mn_yO_{3-\delta}$ series increases with the Mn-content in both oxidising and reducing atmospheres (Fig. 6b). Furthermore, the conductivity in air is up to one order of magnitude higher compared to humidified 5%H_2-Ar. It should be also noted that $PCCM_{0.8}$ sample is not stable in 5%H_2-Ar atmosphere at least at high temperature, undergoing a significant decrease of the conductivity during the time.

3.4. Electrode microstructure

Characteristic SEM images of the electrode–electrolyte interfaces for electrodes with different Mn-composition are illustrated in Fig. 7. Powders of PCCM are made of uniform particles with a homogeneous particle-size distribution in the submicrometric range. One can also see that the grain size of the electrodes increases with the Mn content (Fig. 7). This is explained by the lower sintering temperature of samples containing Mn. In fact, ceramic pellets

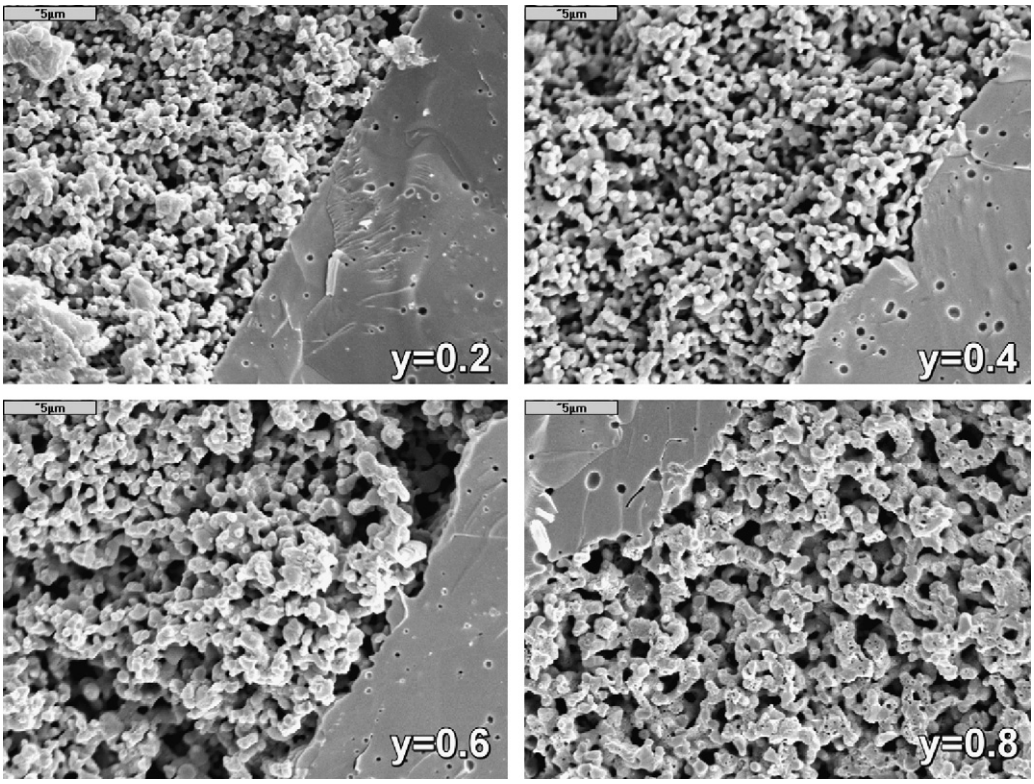

Fig. 7. SEM images showing the microstructure of electrode–electrolyte interfaces for $Pr_{0.7}Ca_{0.3}Cr_{1-y}Mn_yO_{3-\delta}$.

with higher Mn composition exhibit higher relative density and also larger grain size. Therefore, Mn-substitution contributes to increase the sinterability and grain growth in $Pr_{0.7}Ca_{0.3}CrO_{3-\delta}$ materials. The electrodes after the electrochemical characterisation under oxidising and reducing conditions show porous and homogeneous microstructure with adequate adherence to the YSZ electrolyte, indicating good thermal compatibility between both materials. The electrode thickness is about 40 μm. No reaction or diffusion region is observed in the electrode–electrolyte interface.

3.5. Polarisation resistances

The ASR values determined under oxidising and reduction conditions are shown in Fig. 8. The minimum values for PCCM correspond to the sample with high Mn-content. However, as previously mentioned, samples with Mn-composition $y > 0.6$ are unstable under reducing conditions (Fig. 5).

In any case, ASR values are rather high compared to other SOFC electrodes, even working at high temperature as 950 °C. Nevertheless, the ASR values obtained from symmetrical measurement under the same gas composition (without chemical potential gradient) can be different to those obtained from fuel cell tests [4], because SOFC operates under an oxygen chemical potential gradient with oxidant and reducing gases in the cathode and anode respectively, and the current across the cell affects the polarisation of both electrodes. Nevertheless, the symmetrical cell electrode measurement is a useful and easy method to compare different materials.

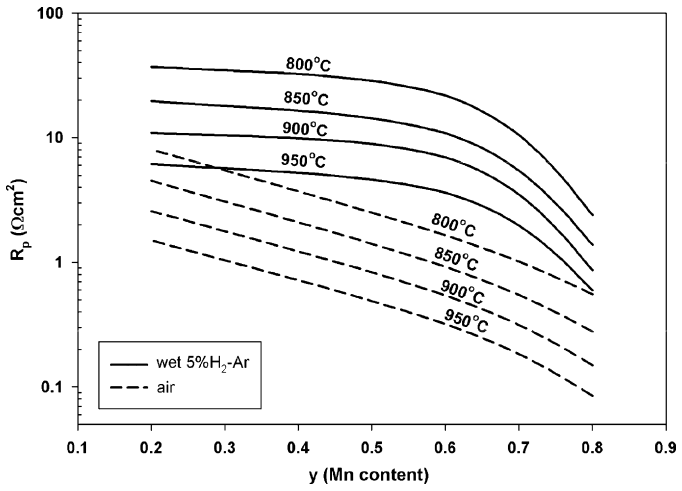

Fig. 8. Area-specific resistance (ASR) values for $Pr_{0.7}Ca_{0.3}Cr_{1-y}Mn_yO_{3-\delta}$ as a function of the Mn-content at different temperatures.

3.6. Fuel cell tests

Two symmetrical fuel cells were assembled using $PCCM_{0.4}$ (selected composition of Mn that seems to be stable under reducing condition) and $PCCM_{0.8}$ (composition of Mn that renders minimum values of ASR, Fig. 8) and the performances were evaluated using different fuels (Fig. 9) and as a function of the measured temperature for the $PCCM_{0.4}$-based system (Fig. 10).

As expected from the ASR measurements, the performance values obtained were rather modest, in both cases, and the highest one was obtained under humidified pure H_2 at 950 °C, rendering 250 and 300 mW cm^{-2} for $PCCM_{0.4}$ and $PCCM_{0.8}$ respectively, Fig. 9. These values correspond with 70% and 84% of the maximum theoretical power density [8], respectively. The $PCCM_{0.8}$-based system exhibits higher performance as expected from its corresponding symmetrical ASR values, Fig. 8. However $PCCM_{0.8}$ shows a decrease of about 6% in just 30 min under pure hydrogen and a significant performance loss of more than 30% after one day of cycling under oxidising (air) and reducing conditions (5%H_2-Ar). Whereas stability is the main feature for the $PCCM_{0.4}$-based system, in the

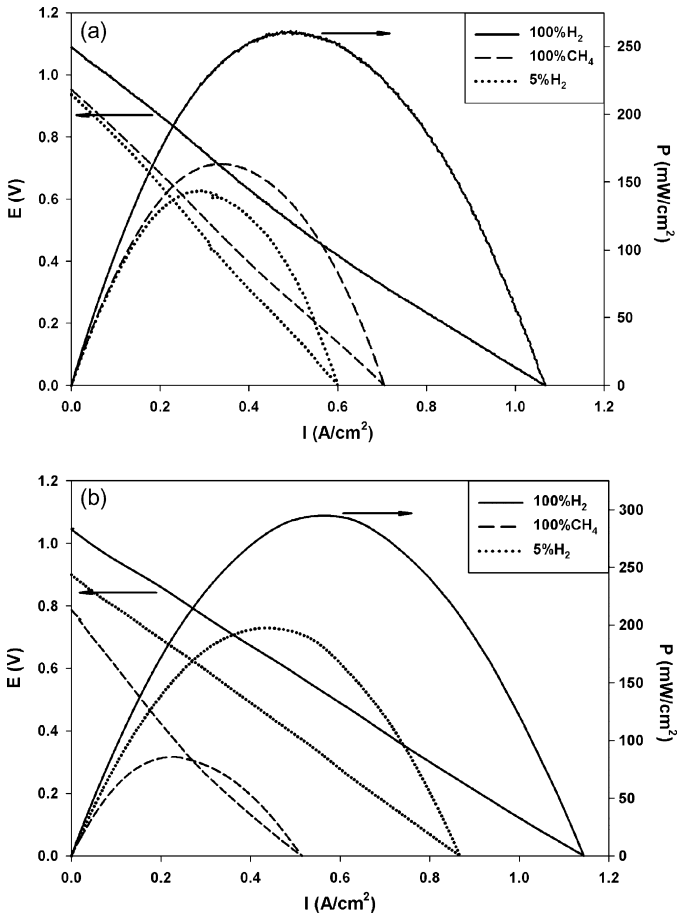

Fig. 9. Fuel cell test of (a) $PCCM_{0.4}$/YSZ/$PCCM_{0.4}$ and (b) $PCCM_{0.8}$/YSZ/$PCCM_{0.8}$ symmetrical cells under different humidified fuels at 950 °C.

same experimental conditions, although with lower performances. More remarkable is the performance under methane, in this system, yielding 160 mW cm^{-2} and OCV of 0.95 V. The lower OCV observed for $PCCM_{0.8}$ is mainly related to the degradation of this material under reducing conditions. Note that the cell is first tested under 5%H_2-Ar, at several temperatures, then under pure hydrogen and finally with methane, and at this stage, the material has been deeply affected by the reducing working conditions.

Although the low performance obtained with other chromite-based materials tested in similar conditions in a previous work [8] was partially attributed to the high sintered microstructure. In the present work, the microstructure and porosity distribution seem to be adequate for an SOFC electrode material (Fig. 7). Thus, the low performance seems to be attributed to the low catalytic activity under reducing conditions as observed from the symmetrical cell measurements, Fig. 8. Note that in this work the electrode was prepared without YSZ composite, hence the triple phase boundary (TPB) area was reduced to the interface between electrode and electrolyte, limiting the achievable performance. Thus an improvement of the performance would be expected using YSZ- or doped-ceria-based composites.

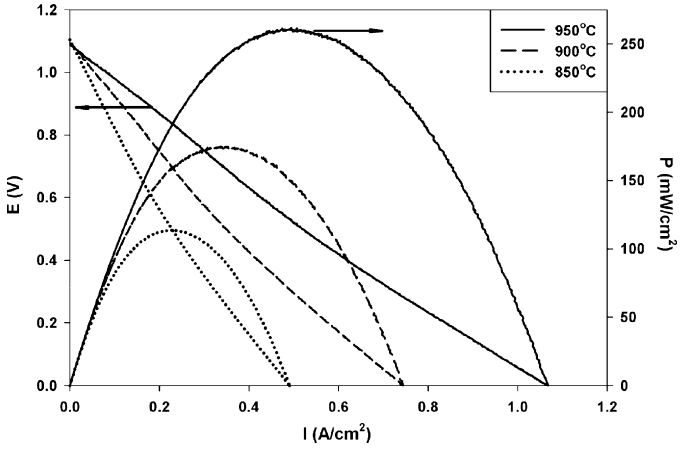

Fig. 10. Fuel cell test of $PCCM_{0.4}$/YSZ/$PCCM_{0.4}$ symmetrical cell under humidified pure hydrogen at several temperatures.

4. Conclusions

In this work the simultaneous use of a based interconnect material as both cathode and anode material for SOFCs has been investigated. Its application is restricted at high temperatures due to the high area-specific resistance values. Samples with high Mn-content exhibited the lower area-specific resistances, however electrochemical and XRD studies and cell characterisation shown that samples with Mn-content higher than 0.6 are unstable under 5%H_2-Ar, e.g. performance losses of more than 30% in one day were observed for $PCCM_{0.8}$-based symmetrical fuel cell.

An alternative synthetic route based in freeze-drying precursors allows obtaining powder with smaller grains size and at lower sintering temperatures compared to traditional solid state reaction.

Finally, $PCCM_{0.4}$/YSZ/$PCCM_{0.4}$ fuel cell achieved performances of 250 and 160 mW cm^{-2} at 950 °C using humidified H_2 and CH_4, respectively as fuels, and air as oxidant.

Acknowledgements

This work was supported by the Spanish Research program (MAT2007-60127). The authors wish to thank "Ministerio de Educación y Ciencia" for a "Juan de La Cierva" fellowship (D. M.-L. and J. P.-M.) and a "Ramón y Cajal" fellowship (J. C. R-M). A.E.-H also thanks to University of La Laguna for a grant ("Ayudas para estudiantes extranjeros e investigadores latinoamericanos y africanos 2006). The authors are also grateful to Luis Hernández (Department of Inorganic Chemistry, University of La Laguna) for technical assistance.

References

[1] N.Q. Minh, T. Takahashi, Science and Technology of Ceramic Fuel Cells, Elsevier, Amsterdam, 1995.
[2] S.C. Singhal, K. Kendall, High Temperature Solid Oxide Fuel Cells, Elsevier, Oxford, 2004.
[3] J.C. Ruiz-Morales, J. Canales-Vázquez, D. Marrero-López, D. Pérez-Coll, J. Peña-Martínez, P. Núñez, J. Power Sources 177 (1) (2008) 154–160.
[4] J.C. Ruiz-Morales, J. Canales-Vázquez, J. Peña-Martínez, D. Marrero-López, P. Núñez, Electrochim. Acta 52 (2006) 278–284.
[5] D.M. Bastidas, S. Tao, J.T.S. Irvine, J. Mater. Chem. 16 (2006) 1603–1605.
[6] S.P. Jiang, L. Zhang, Y. Zhang, J. Mater. Chem. 17 (2007) 2627–2635.
[7] L. Zhang, S.P. Jiang, C.S. Cheng, Y. Zhang, J. Electrochem. Soc. 154 (2007) B577–B582.
[8] J.C. Ruiz-Morales, H. Lincke, D. Marrero-López, J. Canales-Vázquez, P. Núñez, Bol. Soc. Esp. Ceram. V 46 (2007) 218–223.
[9] J.C. Ruiz-Morales, J. Canales-Vázquez, B. Ballesteros, J. Peña-Martínez, D. Marrero-López, J.T.S. Irvine, P. Núñez, J. Eur. Ceram. Soc. 27 (2007) 4223–4227.
[10] J. Canales-Vázquez, J.C. Ruiz-Morales, D. Marrero-López, J. Peña-Martínez, P. Núñez, P. Gómez-Romero, J. Power Sources 171 (2007) 552–557.
[11] J.C. Ruiz-Morales, J. Canales-Vázquez, H. Lincke, J. Peña-Martínez, D. Marrero-López, D. Pérez-Coll, J.T.S. Irvine, P. Núñez, Bol. Soc. Esp. Ceram. V 47 (4) (2008) 183–188.
[12] J. Canales-Vázquez, J.C. Ruiz-Morales, B. Ballesteros, D. Marrero-López, John T.S. Irvine, Bol. Soc. Esp. Ceram. V 46 (2007) 304–310.
[13] J. Sfeir, J. Van Herle, A.J. McEvoy, in: P. Stevens (Ed.), Proceedings of the Third European Solid Oxide Fuel Cell Forum, Ulf Bossel, Nantes-France, 1998, pp. 267–276.
[14] J. Sfeir, P.A. Buffat, P. Möckli, N. Xanthopoulos, R. Vasquez, H.J. Mathieu, J. Van Herle, K.R. Thampi, J. Catal. 202 (2001) 229–244.
[15] J. Liu, B.D. Madsen, Z. Ji, S.A. Barnett, Electrochem. Solid-State Lett. 5 (6) (2002) A122–A124.

[16] S. Tao, J.T.S. Irvine, Nat. Mater. 2 (2003) 320–323.
[17] S. Tao, J.T.S. Irvine, J. Electrochem. Soc. 151 (2004) A252–A259.
[18] G. Kim, G. Corre, J.T.S. Irvine, J.M. Vohs, R.J. Gorte, Electrochem. Solid State Lett. 11 (2) (2008) B16–B19.
[19] Z. Liu, D. Dong, X. Huang, Z. Lü, Y. Sui, X. Wang, J. Miao, Z. Xiang Shen, W. Su, Electrochem. Solid-State Lett. 8 (5) (2005) A250–A252.
[20] T.R. Amstrong, J.W. Stevenson, K. Hasinska, D.E. McCready, J. Electrochem. Soc. 145 (1998) 4282.
[21] J. Rodriguez-Carvajal, FULLPROF Program, Collected Abstracts of Powder Diffraction Meeting, Toulouse, France, 1990, pp. 127–128.
[22] J. Rodríguez-Carvajal, T. Roisnel, "FullProf.98 and WinPLOTR: New Windows 95/NT Applications for Diffraction", Newsletter no. 20 (May–August) summer 1998.
[23] D. Pérez-Coll, P. Núñez, J.R. Frade, J.C.C. Abrantes, Electrochim. Acta 48 (2003) 1551–1557.
[24] D. Marrero-López, J. Peña-Martínez, J.C. Ruiz-Morales, D. Pérez-Coll, M.C. Martín-Sedeño, P. Núñez, Solid State Ionics 178 (2007) 1366–1378.
[25] A. El-Himri, D. Marrero-López, P. Núñez, J. Solid State Chem. 177 (2004) 3219–3223.
[26] S. Tao, J.T.S. Irvine, Chem. Mater. 18 (23) (2006) 5453–5460.